

MINT: Multimodal Imaging-to-Speech Knowledge Transfer for Early Alzheimer’s Screening

Vrushank Ahire^{*1}, Yogesh Kumar^{*1}, Anouck Girard², and M. A. Ganaie¹

¹ Department of CSE, Indian Institute of Technology Ropar, Punjab, India
{2022csb1002, yogesh.23csz0014, mudasir}@iitrpr.ac.in

² Embry-Riddle Aeronautical University, FL, USA
girarda3@erau.edu

Abstract. Alzheimer’s disease is a progressive neurodegenerative disorder in which mild cognitive impairment (MCI) marks a critical transition between aging and dementia. Neuroimaging modalities, such as structural MRI, provide biomarkers of this transition; however, their high costs and infrastructure needs limit their deployment at a population scale. Speech analysis offers a non-invasive alternative, but speech-only classifiers are developed independently of neuroimaging, leaving decision boundaries biologically ungrounded and limiting reliability on the subtle CN-versus-MCI distinction. We propose MINT (Multimodal Imaging-to-Speech Knowledge Transfer), a three-stage cross-modal framework that transfers biomarker structure from MRI into a speech encoder at training time. An MRI teacher, trained on 1,228 subjects, defines a compact neuroimaging embedding space for CN-versus-MCI classification. A residual projection head aligns speech representations to this frozen imaging manifold via a combined geometric loss, adapting speech to the learned biomarker space while preserving imaging encoder fidelity. The frozen MRI classifier, which is never exposed to speech, is applied to aligned embeddings at inference and requires no scanner. Evaluation on ADNI-4 shows aligned speech achieves performance comparable to speech-only baselines (AUC 0.720 vs 0.711) while requiring no imaging at inference, demonstrating that MRI-derived decision boundaries can ground speech representations. Multimodal fusion improves over MRI alone (0.973 vs 0.958). Ablation studies identify dropout regularization and self-supervised pretraining as critical design decisions. To our knowledge, this is the first demonstration of MRI-to-speech knowledge transfer for early Alzheimer’s screening, establishing a biologically grounded pathway for population-level cognitive triage without neuroimaging at inference.

Keywords: Alzheimer’s disease · mild cognitive impairment · speech biomarkers · knowledge transfer · multimodal learning · neuroimaging

1 Introduction

Alzheimer’s disease (AD) and related dementias affect over 55 million people worldwide, and mild cognitive impairment (MCI) represents the last clinically

* Equal contribution.

actionable stage before dementia [1]. Early detection improves prognosis, yet population-scale screening remains challenging. Established biomarkers such as hippocampal atrophy on structural MRI and amyloid-related indices require expensive hardware, specialised expertise, and infrastructure often unavailable in primary care or low-resource settings [2, 3].

Deep learning on structural MRI has produced reliable classifiers for MCI and AD. Convolutional architectures trained on hippocampal subregions and whole-brain tissue maps demonstrate strong performance on cohorts such as the Alzheimer’s Disease Neuroimaging Initiative (ADNI) [4, 5]. Self-supervised and contrastive strategies further enhance MRI representations under label scarcity typical of clinical neuroimaging datasets [6, 7]. Multimodal teacher models combining MRI and PET have been used to supervise MRI-only students, achieving performance close to systems without requiring PET at inference [8, 9]. Speech has emerged as a scalable, non-invasive biomarker. Narrative and verbal fluency tasks reveal lexical, prosodic, and articulatory changes associated with early neurodegeneration [10, 11]. Acoustic representations combined with self-supervised speech encoders achieve competitive results on DementiaBank and ADReSS [12, 13]. Recent approaches integrate Wav2Vec-style encoders with large language model features to improve acoustic and transcription-based pipelines [14, 15].

Despite this progress, two limitations remain. First, most studies focus on the AD-versus-cognitively-normal distinction, whereas subtler transition from cognitively normal to MCI remains less explored [3, 16]. Second, speech-only models are developed independently of imaging biomarkers, limiting biological grounding and interpretability. Multimodal fusion mitigates this issue [17, 18], but requires all modalities at test time, restricting deployment in resource-limited settings. Knowledge distillation [19] and cross-modal representation learning offer an alternative: training a student to replicate a teacher’s latent space enables unimodal inference after multimodal supervision. This paradigm has been explored in imaging-only settings [20] and in audio–visual and vision–language domains [21, 22]. However, grounding speech in a neuroimaging-derived biomarker space through cross-modal distillation has not been investigated for MCI detection.

We address this gap with MINT, which uses a pretrained MRI classifier to define a biomarker space predictive of MCI and trains a speech projection head to align with it. This enables speech-based inference without imaging at test time. Our contributions are:

- A three-stage teacher–student framework comprising self-supervised speech pretraining, an MRI teacher defining a biomarker space, and a cross-modal projection of speech into this space.
- A cross-modal alignment strategy that enables speech models to inherit imaging-derived decision structure while operating independently at inference.
- Systematic ablations demonstrating the importance of projection-head regularization and self-supervised pretraining for stable knowledge transfer.
- Strong performance on CN-versus-MCI classification, where aligned speech achieves comparable results to speech-only baselines while requiring no imaging at inference, and fusion improves over MRI alone.

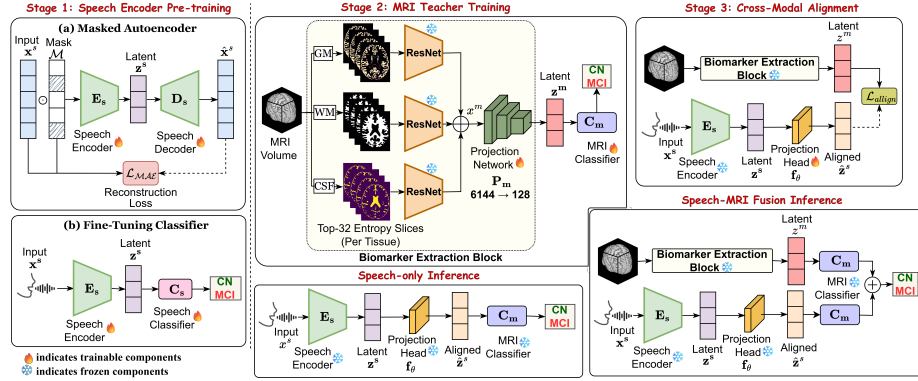


Fig. 1. Overview of the three-stage MINT framework. In Stage 1, a speech encoder is pretrained using masked autoencoding and then fine-tuned for CN–MCI classification. In Stage 2, an MRI teacher is trained via tissue-stratified feature extraction to learn a 128-dimensional biomarker embedding space. In Stage 3, a projection head aligns speech embeddings to the frozen MRI space, enabling speech-only inference as well as multimodal fusion.

2 Methodology

2.1 Problem Setup and Notation

Let $\mathbf{x}^s \in \mathbb{R}^{209}$ denote acoustic features from speech, and $\mathbf{x}^m \in \mathbb{R}^{6144}$ MRI-derived features. Using 266 paired training subjects, we learn a speech encoder and projection head that distinguish CN from MCI without requiring MRI at inference. We denote fine-tuned speech latents as $\mathbf{z}^s \in \mathbb{R}^{128}$, MRI biomarker embeddings as $\mathbf{z}^m \in \mathbb{R}^{128}$, and aligned speech as $\hat{\mathbf{z}}^s = f_\theta(\mathbf{z}^s)$. The shared 128-dimensional bottleneck makes alignment well-posed and reduces overfitting risk. Figure 1 illustrates the three-stage pipeline.

2.2 Stage 1: Speech Encoder Pretraining and Fine-tuning

Self-supervised pretraining. Given that labeled speech data for MCI are limited ($N \approx 222$), we first pretrain the speech encoder E_s on a pool of 14,235 unlabeled acoustic feature samples using a masked autoencoder (MAE) [23] objective inspired by BERT [24]. Pretraining on unlabeled data is particularly important here because the encoder must learn a rich, general-purpose acoustic representation before being exposed to the small labeled set; without this initialization, supervised fine-tuning on the small labeled set risks fitting noise rather than clinically meaningful patterns.

A random subset of the 209 input features is masked; the encoder-decoder E_s, D_s reconstructs the original input \mathbf{x} as $\hat{\mathbf{x}}$ via:

$$\mathcal{L}_{\text{MAE}} = \frac{\sum_{i \in \mathcal{M}} (x_i - \hat{x}_i)^2}{|\mathcal{M}|} + \lambda_c \cdot (1 - \cos(\mathbf{x}, \hat{\mathbf{x}})), \quad (1)$$

where \mathcal{M} denotes the set of masked indices and λ_c is tuned by Bayesian HPO (Optuna [25]) together with architecture hyperparameters. The cosine term in Eq. (1) preserves directional structure in the latent space, which improves stability during later cross-modal alignment. Intuitively, two embeddings that point in the same direction in \mathbb{R}^{128} will respond similarly to a linear classifier; encouraging this property during pretraining means the encoder already organizes features in a way that is compatible with the downstream alignment objective.

Supervised fine-tuning. The pretrained encoder E_s is fine-tuned for CN-vs-MCI classification by attaching a single linear head $C_s : \mathbb{R}^{128} \rightarrow \mathbb{R}^2$ and optimizing with soft cross-entropy. Given the class imbalance ($\approx 2:1$) and small dataset, we apply Mixup augmentation [26] with $\alpha=0.3$ and label smoothing $\varepsilon=0.10$. Mixup creates convex combinations of training examples and their labels, which has been shown to reduce overconfident predictions and improve calibration under class imbalance [26]; label smoothing provides a complementary regularization effect by preventing the model from assigning zero probability to non-target classes. Discriminative learning rates are used: 10^{-4} for the freshly initialized head and 10^{-5} for the pretrained encoder. Using a lower learning rate for the encoder preserves the general acoustic structure learned during pretraining while allowing the head to adapt quickly to the classification boundary. To address the class imbalance, inverse-frequency weighting is applied with $w_c = N/(2N_c)$.

2.3 Stage 2: MRI Feature Extraction and Teacher Training

Feature extraction. Raw T1-weighted MRI volumes are preprocessed with N4 bias-field correction, skull stripping, and registration to MNI space using ANTs SyN [27]. Tissue segmentation (CSF, gray matter, white matter) is performed using the Atropos algorithm [28]. For each tissue type, the 32 axial slices with the highest tissue-probability-weighted entropy are selected. An ImageNet-pretrained ResNet-50 [29] extracts 2048-d feature vector per slice, which is averaged across slices [30]. Concatenating the three tissue vectors yields $\mathbf{x}^m \in \mathbb{R}^{6144}$ for each subject. Tissue stratification is motivated by compartment-specific neurodegenerative patterns: gray matter atrophy is an early marker of MCI, whereas white matter and CSF alterations provide supporting information regarding structural decline. [2]. Entropy-based slice selection prioritizes regions with high tissue contrast and excludes near-uniform background areas.

MRI teacher. A deep MLP with monotonically decreasing hidden widths $6144 \rightarrow h_1 \rightarrow \dots \rightarrow h_k \rightarrow 128$ is trained to classify CN vs. MCI. The architecture is factored into a projection network $P_m : \mathbb{R}^{6144} \rightarrow \mathbb{R}^{128}$ (the ‘‘biomarker space’’) and a linear classifier $C_m : \mathbb{R}^{128} \rightarrow \mathbb{R}^2$. This factored design is deliberate: by separating the compression step from the classification step, we obtain a reusable embedding space that the speech model can later target directly. If the two functions were entangled in a single monolithic network, there would be no well-defined intermediate representation for the speech model to align to. The depth k and widths $\{h_i\}$ are selected by Optuna Bayesian HPO (60 trials, TPE sampler, MedianPruner). The MRI teacher is trained on 1,228 labeled MRI subjects, providing a substantially larger supervised signal than is available for speech

alone. This larger training set is one reason the MRI teacher serves as a reliable reference: its biomarker space is learned from enough examples to generalize well, making it a stable target for the alignment stage. After training, both P_m and C_m are *frozen*; only these frozen weights are used in Stage 3. Freezing is essential: it ensures that the MRI biomarker space does not shift during alignment training, so that the projection head is forced to move speech embeddings toward MRI rather than the reverse.

2.4 Stage 3: Cross-Modal Alignment

The key novelty of MINT is the alignment stage. The frozen speech encoder (from Stage 1) produces \mathbf{z}^s ; a trainable projection head $f_\theta : \mathbb{R}^{128} \rightarrow \mathbb{R}^{96} \rightarrow \mathbb{R}^{128}$ maps it to an aligned embedding $\hat{\mathbf{z}}^s = f_\theta(\mathbf{z}^s)$. The head uses a single hidden layer with BatchNorm, GELU activation, Dropout(0.6), and a residual skip connection weighted by 0.1 to ensure gradient flow. Keeping the projection head deliberately small is a conscious regularisation choice: with only 74 MCI subjects among the 266 paired training subjects, a larger head would have enough capacity to memorise subject-specific idiosyncrasies rather than learn a general speech-to-MRI mapping. The residual connection allows the head to default to a near-identity mapping early in training, giving the optimiser a stable starting point before the alignment loss guides it toward the MRI space.

We align normalised embeddings using a two-term loss:

$$\mathcal{L}_{\text{align}} = \lambda_{\text{mse}} \|\hat{\mathbf{z}}_n^s - \mathbf{z}_n^m\|^2 + \lambda_{\text{cos}} (1 - \cos(\hat{\mathbf{z}}_n^s, \mathbf{z}_n^m)), \quad (2)$$

where subscript n denotes ℓ_2 -normalisation. The MSE term penalises magnitude discrepancies and the cosine term penalises directional misalignment; together they enforce that $\hat{\mathbf{z}}^s$ occupies precisely the same region of \mathbb{R}^{128} as \mathbf{z}^m , so the frozen linear classifier C_m can be applied to speech without modification. The core mechanism of MINT relies on the fact that C_m , having been trained on \mathbf{z}^m , has already established decision boundaries in the MRI biomarker space. By mapping $\hat{\mathbf{z}}^s$ into this space, the speech model can inherit these boundaries instead of rediscovering them from a limited labeled set. Using ℓ_2 -normalised embeddings for both terms ensures that the loss is not dominated by subjects with high-magnitude embeddings, which promotes consistent alignment across the CN and MCI classes. Only f_θ is updated during Stage 3. Loss weights ($\lambda_{\text{mse}}, \lambda_{\text{cos}}$) and learning rate are selected by a stratified 5-fold cross-validation grid search on the training split.

Inference. In the *speech-only* scenario, predictions are obtained as

$$\hat{p} = \text{softmax}(C_m(f_\theta(E_s(\mathbf{x}^s)))), \quad (3)$$

requiring no MRI. In the *paired* scenario, logit-level fusion averages the logits from $C_m(\mathbf{z}^m)$ and $C_m(\hat{\mathbf{z}}^s)$, exploiting complementary signal from both modalities. The two scenarios directly correspond to two different deployment contexts: a community screening setting where only a smartphone recording is available, and a memory clinic where MRI has already been acquired. MINT is designed to be useful in both.

3 Experiments and Results

3.1 Dataset and Unified Evaluation Protocol

Dataset. We use ADNI-4 Storyteller [31] data comprising: (1) 14,235 unlabeled speech recordings for MAE pretraining; (2) 1,228 MRI-only subjects (677 CN, 551 MCI) for teacher training; (3) 266 paired subjects (187 CN, 79 MCI) for alignment. Speech features are 209-d acoustic descriptors (pitch, MFCCs, formants, jitter, shimmer, etc.). MRI features (6144-d) are tissue-stratified ResNet-50 embeddings.

Unified evaluation. Experiments share a single stratified 70/15/15 split ($seed = 42$), yielding a test set of 40 subjects (28 CN, 12 MCI). All methods are evaluated on identical test subjects to control for sampling variability. We use AUC-ROC as the primary metric for class imbalance. With $N = 40$ test subjects, 95% bootstrap confidence intervals are ± 0.08 , so differences should be viewed as directional.

Implementation. All models are trained using AdamW with cosine decay ($T_0 = 50$) for up to 200 epochs, with early stopping based on validation AUC (patience 30). Experiments are conducted on a single NVIDIA A100 GPU (40GB).

3.2 Main Results

Table 1 presents a comparison of ML models: Random Forest (RF), Support Vector Machine (SVM), Multi-Layer Perceptron (MLP), XGBoost, and Logistic Regression (LR) alongside the proposed MINT variants on a unified test set. The

Table 1. Test-set results (40 subjects, 28 CN / 12 MCI). †: requires MRI at inference. All methods on identical split.

| Category | Method | AUC \uparrow |
|---------------------|--------------------------------------|----------------|
| Speech baselines | RF on acoustic features [32] | 0.711 |
| | SVM (RBF) [33] | 0.705 |
| | MLP from scratch [34] | 0.661 |
| | XGBoost [35] | 0.613 |
| | LR on acoustic features [36] | 0.580 |
| MINT Stage 2 † | MRI teacher (CV: 0.780 ± 0.029) | 0.958 |
| MINT (ours) | Aligned speech | 0.720 |
| | Fusion † | 0.973 |

speech-only baselines trained on 186 subjects achieve AUCs between 0.580 and 0.711. RF achieves the highest AUC (0.711), followed by SVM (0.705). These results indicate that acoustic features provide discriminative information for early MCI detection, although performance remains modest. The MRI teacher, trained on 1,228 subjects, achieves a 5-fold cross validation AUC of 0.780 ± 0.029 and a test AUC of 0.958. The improvement reflects the larger training cohort and the stronger signal from structural neuroimaging.

After alignment, MINT speech achieves an AUC of 0.720. Critically, this model uses a classifier trained entirely on MRI without ever seeing speech labels, yet performs comparably to the best speech baseline (0.711). This 0.009 difference falls within the 95% CI (± 0.08), indicating statistical equivalence while demonstrating successful cross-modal transfer. Thus, the teacher establishes a stable embedding space for speech alignment, enabling speech representations to inherit imaging-derived decision structure rather than learning it independently. Finally, logit-

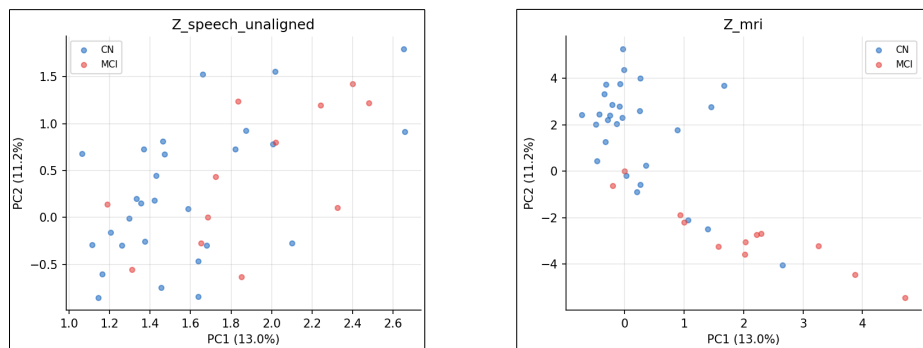


Fig. 2. PCA visualization shows higher class overlap in speech embeddings, whereas MRI embeddings display better separation between CN (blue) and MCI (red). This modality gap motivates the cross-modal alignment objective.

level fusion achieves an AUC of 0.973, exceeding the MRI teacher alone (0.958). The performance gain indicates that aligned speech preserves complementary modality-specific variation, enriching the combined representation. Additionally, Figure 2 visually depicts this effect by mapping the modality gap using PCA.

3.3 Ablation Studies

Table 2 isolates each MINT component. Δ Fusion quantifies impact on multimodal performance relative to MINT default (0.973).

Table 2. Ablation study on unified test set. All variants use identical split as Table 1.

| Variant | Speech AUC | Fusion AUC | Δ Fusion |
|--|--------------|--------------|-----------------|
| MINT default | 0.720 | 0.973 | — |
| MSE only ($\lambda_{\text{cos}}=0$) | 0.717 | 0.955 | -0.018 |
| Cosine only ($\lambda_{\text{mse}}=0$) | 0.711 | 0.937 | -0.036 |
| Larger head (hidden 128) | 0.708 | 0.914 | -0.059 |
| No pretrain (scratch) | 0.667 | 0.907 | -0.066 |
| No dropout (proj. head) | 0.658 | 0.857 | -0.116 |

Self-supervised pretraining. Replacing MAE-pretrained encoder with random initialization reduces speech AUC by 0.053 (0.667 vs. 0.720) and fusion AUC by 0.066 (0.907 vs. 0.973)—the largest degradation in speech-only performance. The result validates the pretraining rationale: the MAE objective on 14,234 unlabeled feature samples yields an encoder capable of meaningful alignment with only 186 labeled subjects. A randomly initialised encoder lacks the general acoustic structure needed for the projection head to find the MRI biomarker space.

Dropout regularization. Removing Dropout(0.6) from the projection head causes the largest overall degradation: fusion AUC drops 0.116 (0.857 vs. 0.973). With only 55 MCI-positive training subjects, strong dropout is necessary to prevent memorization of subject-specific artifacts and promote generalization.

Loss function design. MSE-only achieves speech AUC 0.717 and fusion 0.955; cosine-only achieves 0.711 and 0.937. Both fall below combined default (0.720/0.973), confirming MSE and cosine address complementary aspects of embedding geometry. The combined loss provides the best alignment at both the speech-AUC and fusion levels.

Projection head capacity. Increasing hidden dimension from 96 to 128 reduces speech AUC (0.708) and fusion AUC (0.914), consistent with overfitting. The default 96-d head balances model capacity and overfitting.

4 Discussion and Conclusion

An MRI-trained classifier achieves an AUC of 0.720 on aligned speech using a frozen C_m trained without speech features. MINT speech outperforms RF speech (0.711), suggesting that MRI-grounded representations provide complementary discriminative information beyond speech-only training. The MRI branch is trained on 1,228 subjects, yielding a stable representation used for distillation to the speech branch with 266 paired subjects. This imbalance occurs because imaging cohorts are generally larger than multimodal datasets. However, our findings suggest that large-scale unimodal training can regularize learning in smaller multimodal contexts. Multimodal fusion achieves an AUC of 0.973, exceeding the MRI-only model. Ablation experiments show performance drops when projection head regularization or MAE pretraining is removed, indicating the role of embedding stability and initialization under limited paired data.

The paired cohort size ($N = 266$) limits alignment quality and produces wide confidence intervals on the 40-subject test set ($\approx \pm 0.08$ AUC). The study is limited to a single cohort; broader evaluation across sites and demographic groups is needed to establish generalizability. Knowledge distillation and contrastive objectives showed limited gains due to the small paired dataset; larger multimodal cohorts could improve alignment. Future work will expand MINT to multi-site cohorts, and explore temporally-aware speech modeling for improved cognitive decline detection. Self-supervised cross-modal pretraining may stabilize alignment with limited paired data. Overall, MINT offers a scalable, biology-based method for speech-based cognitive screening without needing imaging at inference.

Code availability. Code will be made publicly available upon acceptance.

References

1. World Health Organization. *Global status report on the public health response to dementia*. (2021).
2. Jack Jr, Clifford R., et al. NIA-AA research framework: toward a biological definition of Alzheimer’s disease. *Alzheimer’s & Dementia* 14.4 (2018): 535-562.
3. Raza, Muhammad Liaquat, et al. Advancements in deep learning for early diagnosis of Alzheimer’s disease using multimodal neuroimaging: challenges and future directions. *Frontiers in Neuroinformatics* 19 (2025): 1557177.
4. Dong, Xinxiu, et al. Convolutional neural network models of structural MRI for discriminating categories of cognitive impairment: a systematic review and meta-analysis. *BMC Neurology* 25.1 (2025): 400.
5. Yuan, Zengbei, et al. Magnetic resonance radiomics-based deep learning model for diagnosis of Alzheimer’s disease. *Digital Health* 11 (2025): 20552076251337183.
6. Thrasher, Jacob, et al. TE-SSL: time and event-aware self supervised learning for Alzheimer’s disease progression analysis. *International Conference on Medical Image Computing and Computer-Assisted Intervention*. Cham: Springer Nature Switzerland, 2024.
7. Li, Zhiyuan, et al. Joint self-supervised and supervised contrastive learning for multimodal MRI data: Towards predicting abnormal neurodevelopment. *Artificial intelligence in medicine* 157 (2024): 102993.
8. Kwak, Min Gu, et al. A cross-modal mutual knowledge distillation framework for Alzheimer’s disease diagnosis: Addressing incomplete modalities. *IEEE Transactions on Automation Science and Engineering* (2025).
9. Li, Fan, et al. Brain-Heart-Gut Guided Multi-constraint Knowledge Distillation for Early Alzheimer’s Disease Diagnosis. *International Conference on Medical Image Computing and Computer-Assisted Intervention*. Cham: Springer Nature Switzerland, 2025.
10. Fraser, Kathleen C., Jed A. Meltzer, and Frank Rudzicz. Linguistic features identify Alzheimer’s disease in narrative speech. *Journal of Alzheimer’s disease* 49.2 (2015): 407-422.
11. Chandler, Chelsea, et al. An explainable machine learning model of cognitive decline derived from speech. *Alzheimer’s & Dementia: Diagnosis, Assessment & Disease Monitoring* 15.4 (2023): e12516.
12. Zhu, Youxiang, et al. Wavbert: Exploiting semantic and non-semantic speech using wav2vec and bert for dementia detection. *Interspeech*. Vol. 2021. 2021.
13. Li, Changye, et al. Useful blunders: Can automated speech recognition errors improve downstream dementia classification?. *Journal of biomedical informatics* 150 (2024): 104598.
14. Chlasta, Karol, Piotr Struzik, and Grzegorz M. Wójcik. Enhancing dementia and cognitive decline detection with large language models and speech representation learning. *Frontiers in Neuroinformatics* 19 (2025): 1679664.
15. Chi, Lei, et al. Predicting Cognitive Decline: A Multimodal AI Approach to Dementia Screening from Speech. *2025 IEEE International Conference on AI and Data Analytics (ICAD)*. IEEE, 2025.
16. Ding, Kewen, et al. Speech based detection of Alzheimer’s disease: a survey of AI techniques, datasets and challenges. *Artificial Intelligence Review* 57.12 (2024): 325.
17. Lin, Kaiying, and Peter Y. Washington. Multimodal deep learning for dementia classification using text and audio. *Scientific Reports* 14.1 (2024): 13887.

18. Huang, Weijie, and Ni Shu. AI-powered integration of multimodal imaging in precision medicine for neuropsychiatric disorders. *Cell Reports Medicine* 6.5 (2025).
19. Hinton, Geoffrey, Oriol Vinyals, and Jeff Dean. Distilling the knowledge in a neural network. *arXiv preprint arXiv:1503.02531* (2015).
20. Kunanbayev, Kassymzhomart, Vyacheslav Shen, and Dae-Shik Kim. Training ViT with limited data for Alzheimer’s disease classification: an empirical study. *International Conference on Medical Image Computing and Computer-Assisted Intervention*. Cham: Springer Nature Switzerland, 2024.
21. Radford, Alec, et al. Learning transferable visual models from natural language supervision. *International conference on machine learning*. PmLR, 2021.
22. Elizalde, Benjamin, et al. Clap learning audio concepts from natural language supervision. *ICASSP 2023-2023 IEEE International Conference on Acoustics, Speech and Signal Processing (ICASSP)*. IEEE, 2023.
23. Yoon, Jinsung, et al. Vime: Extending the success of self-and semi-supervised learning to tabular domain. *Advances in neural information processing systems* 33 (2020): 11033-11043.
24. Devlin, Jacob, et al. Bert: Pre-training of deep bidirectional transformers for language understanding. *Proceedings of the 2019 conference of the North American chapter of the association for computational linguistics: human language technologies, volume 1 (long and short papers)*. 2019.
25. Akiba, Takuya, et al. Optuna: A next-generation hyperparameter optimization framework. *Proceedings of the 25th ACM SIGKDD international conference on knowledge discovery & data mining*. 2019.
26. Zhang, Hongyi, et al. mixup: Beyond empirical risk minimization. *arXiv preprint arXiv:1710.09412* (2017).
27. Avants, Brian B., et al. A reproducible evaluation of ANTs similarity metric performance in brain image registration. *Neuroimage* 54.3 (2011): 2033-2044.
28. Avants, Brian B., et al. An open source multivariate framework for n-tissue segmentation with evaluation on public data. *Neuroinformatics* 9.4 (2011): 381-400.
29. He, Kaiming, et al. Deep residual learning for image recognition. *Proceedings of the IEEE conference on computer vision and pattern recognition*. 2016.
30. Tanveer, Muhammad, et al. Classification of Alzheimer’s disease using ensemble of deep neural networks trained through transfer learning. *IEEE Journal of Biomedical and Health Informatics* 26.4 (2021): 1453-1463.
31. Rivera Mindt, Mónica, et al. The Alzheimer’s Disease Neuroimaging Initiative-4 (ADNI-4) Engagement Core: A culturally informed, community-engaged research (CI-CER) model to advance brain health equity. *Alzheimer’s & Dementia* 20.12 (2024): 8279-8293.
32. Breiman, Leo. Random forests. *Machine learning* 45.1 (2001): 5-32.
33. Cortes, Corinna, and Vladimir Vapnik. Support-vector networks. *Machine learning* 20.3 (1995): 273-297.
34. Rumelhart, David E., Geoffrey E. Hinton, and Ronald J. Williams. Learning representations by back-propagating errors. *nature* 323.6088 (1986): 533-536.
35. Chen, Tianqi, and Carlos Guestrin. XGBoost: A scalable tree boosting system. *Proceedings of the 22nd ACM SIGKDD International Conference on Knowledge Discovery and Data Mining*. 2016.
36. Hosmer Jr, David W., Stanley Lemeshow, and Rodney X. Sturdivant. *Applied logistic regression*. John Wiley & Sons, 2013.